NMR Solution Structure and Receptor Peptide Binding of the CC Chemokine Eotaxin-2[†,‡]

Kristen L. Mayer and Martin J. Stone*

Department of Chemistry, Indiana University, Bloomington, Indiana 47405-0001

Received March 7, 2000; Revised Manuscript Received May 9, 2000

ABSTRACT: The human CC chemokine eotaxin-2 is a specific agonist for the chemokine receptor CCR3 and may play a role in the recruitment of eosinophils in allergic diseases and parasitic infections. We report the solution structure of eotaxin-2 determined using heteronuclear and triple resonance NMR methods. A family of 20 structures was calculated by hybrid distance geometry-simulated annealing from 854 NOE distance restraints, 48 dihedral angle restraints, and 12 hydrogen bond restraints. The structure of eotaxin-2 (73 amino acid residues) consists of a helical turn (residues 17−20) followed by a 3-stranded antiparallel β-sheet (residues 22−26, 37−41, and 44−49) and an α-helix (residues 54−66). The N-loop (residues 9−16) is packed against both the sheet and the helix with the two conserved disulfide bonds tethering the N-terminal/N-loop region to the β-sheet. The average backbone and heavy atom rmsd values of the 20 structures (residues 7−66) are 0.52 and 1.13 Å, respectively. A linear peptide corresponding to the N-terminal region of CCR3 binds to eotaxin-2, inducing concentration-dependent chemical shift changes or line broadening of many residues. The distribution of these residues suggests that the peptide binds into an extended groove located at the interface between the N-loop and the β2−β3 hairpin. The receptor peptide may also interact with the N-terminus of the chemokine and part of the α-helix. Comparison of the eotaxin-2 structure with those of related chemokines indicates several structural features that may contribute to receptor specificity.

Chemokines (chemotactic cytokines) are a family of small soluble proteins that recruit leukocytes during both normal and pathological inflammatory processes (*1*). Chemokines induce leukocyte migration (chemotaxis) by activating seven transmembrane helix G protein-coupled receptors located on the cell surface (*2*). Thus, inhibition of chemokine−receptor interactions is an attractive and potentially rather general approach to prevention or cure of inflammatory diseases. In addition to their functions in mediating inflammation, some chemokine receptors have been identified as the co-receptors required (in conjunction with CD4) for HIV[1] to infect its target cells (*3*−*6*). Thus, some chemokines can block HIV infection by binding to their native receptors (*6,7*).

There are two main subfamilies of chemokines that are distinguished by whether the first two of four conserved cysteine residues are contiguous (CC or β chemokines) or separated by an intervening amino acid (CXC or α chemokines) (*1*). Two chemokines with alternative cysteine motifs have also been reported; fractalkine has a CX_3C motif (*8*), and lymphotactin has only two of the usual four conserved cysteines (*9*). Three-dimensional structures have been determined for several chemokines from each main subfamily, as well as for fractalkine [reviewed in (*10*)]. Although substantial variations in quaternary structure have been observed, all of the tertiary structures are fairly similar, consisting of a relatively unstructured N-terminal region, an extended "N-loop" region, a three-stranded antiparallel β-sheet, and a C-terminal α-helix. A single turn of helix is often located at the junction between the N-loop and the first β-strand, and disulfide bonds tether the CC, CXC, or CX_3C motif (between the N-terminal and N-loop regions) to the β-sheet. Extensive mutational studies on a variety of chemokines have generally indicated that the N-loop region is important for receptor binding whereas the N-terminal region is required for activation of receptors (*11*−*19*). NMR studies of chemokines in the presence of receptor-derived peptides have suggested that the N-terminal extracellular region of the receptor binds into a groove formed by the N-loop and β-sheet regions of the chemokine (*11, 20*).

The chemokine receptors can also be classified into two subfamilies according to whether they are activated by CC or CXC chemokines (*18*); the receptors are denoted by the prefixes 'CCR' and 'CXCR', respectively. Although the

[†] This work was supported by grants awarded to M.J.S. from the National Institutes of Health (GM 55055 and S10 RR11841), the National Science Foundation (MCB-9600968), and the American Heart Association (Established Investigator Award).

[‡] The coordinates have been deposited with the Protein Data Bank under accession codes 1EIG and 1EIH.

* To whom correspondence should be addressed. Phone: 812-855-6779. Fax: 812-855-8300. E-mail: mastone@indiana.edu.

[1] Abbreviations: 2D, 3D, and 4D, two, three, and four dimensional; CCR, CC chemokine receptor; CXCR, CXC chemokine receptor; COSY, correlation spectroscopy; DSS, 2,2-dimethyl-2-silapentane-5-sulfonate, sodium salt; HIV, human immunodeficiency virus; HMQC, heteronuclear multiple-quantum coherence; HSQC, heteronuclear single-quantum coherence; IL-8, interleukin-8; IPTG, isopropyl-β-D-thiogalactopyranoside; MCP, monocyte chemoattractant protein; NMR, nuclear magnetic resonance; NOE, nuclear Overhauser effect; NOESY, nuclear Overhauser effect spectroscopy; rmsd, root-mean-square deviation; TOCSY, total correlation spectroscopy; TPPI, time-proportional phase incrementation; vMIP-II, viral macrophage-inflammatory protein II.

10.1021/bi000523j CCC: $19.00
Published on Web 06/27/2000

receptors in one subfamily are generally not responsive to chemokines from the other subfamily, there is a much lower level of selectivity within each subfamily (*1, 18, 21*). Thus, most chemokines receptors can be activated by more than one chemokine, and most chemokines can activate more than one receptor.

A notable exception to this paradigm is the eotaxin subgroup of CC chemokines, eotaxin (*22*), eotaxin-2 (*23*), and eotaxin-3 (*24*). These chemokines are potent chemoattractants for eosinophils and basophils and are specific for the receptor CCR3, which is expressed on these cell types (*25, 26*). The overaccumulation of eosinophils (hypereosinophilia) is an important pathological feature of allergic inflammation (e.g., allergic asthma) and parasitic infections and can give rise to tissue damage in a wide variety of organs (*27, 28*). Furthermore, CCR3 is also expressed on brain astrocytes and can support HIV infection, implicating CCR3 as a possible mediator of AIDS-related dementia (*29, 30*). Thus, an understanding of the structural basis of CCR3 recognition by eotaxin subgroup chemokines will be beneficial in developing therapeutic approaches to these diseases.

Although the eotaxin subgroup chemokines have identical receptor specificity, their overall sequence identity is only ~34−38%. In contrast, eotaxin has strikingly high sequence identity (65%) to monocyte chemoattractant protein-1 (MCP-1) which binds and activates the receptors CCR2 and CCR4 but not CCR3 (*1, 21*). Residues that are important for controlling receptor specificity might be expected to be identical between chemokines with the same specificity but different in those that bind to a different receptor. However, only five positions are identical between eotaxin and eotaxin-2 but different in MCP-1, and only one of these residues (Pro-19 in eotaxin, Pro-17 in eotaxin-2, Ser-21 in MCP-1) is located in the functionally important N-loop or N-terminal regions. Thus, sequence comparisons do not lead to any convincing hypotheses to explain the specificity differences. This has prompted us to ask the following questions: (1) Are there any 3D structural features that differ systematically between the eotaxin subgroup chemokines and MCP-1? (2) Are the receptor binding regions of the eotaxin subgroup chemokines limited to the N-loop and N-terminus? To address these questions, we have determined the 3D structure of eotaxin-2 and have studied the interaction of eotaxin-2 with a receptor-derived peptide. The results are presented here along with a discussion of the possible implications for receptor specificity.

MATERIALS AND METHODS

Materials. All reagents were purchased from Sigma (St. Louis, MO), unless otherwise indicated. Oligonucleotides were purchased from Midland Certified Reagent Co. (Midland, TX).

Gene Synthesis and Cloning. A gene encoding the published amino acid sequence of eotaxin-2 (*23*), with the codons optimized for expression in *E. coli*, was synthesized by two rounds of recursive PCR (*31*) from the following six overlapping oligonucleotides (numbered from the 5′- to the 3′-end of the coding strand): oligo-1, GGAATTCCATATGATCGAGGGCCGCGTTGTGATCCCGTCTCCGTGCTGTATGTTC; oligo-2, GTTGTGATCCCGTCTCCGTGCTGTATGTTCTTCGTATCCAAACGTATCCCGGAAAACCGTGTTGTGTCTTAC; oligo-3, AGTGGTAAAAATAACACCCGCCTTCAGGCAGGTAGAACGGGAAGACAGCTGGTAAGACACAACACGGTTTTC; oligo-4, GCGGGTGTTATTTTTACCACTAAAAAG-GGCCAGCAATCCTGCGGTGATCCGAAACAGGAATGGGTTCAGCGCTAC; oligo-5, ACGCGCGCGCGGGGATGCTTTTTTCTGTTTAGCGTCCAGGTTTTTCATGTAGCGCTGAACCCATTCCTGTTTCGG; oligo-6, GGCAAGCTTACTATGCTACAGCACGCGCGCGC-GGGGATGCTTT. The PCR product was restricted with *Nde*I (Promega, Madison, WI) and *Hin*dIII (Promega, Madison, WI) and ligated into a pET-28a plasmid (Novagen, Inc., Madison, WI) C-terminal to the His_6 affinity tag. The synthetic gene sequence encodes an N-terminal factor Xa cleavage site, allowing proteolytic removal of the affinity tag after purification, to yield a protein with a native N-terminus.

Protein Expression and Purification. Eotaxin-2 was overexpressed as inclusion bodies in *E. coli* strain BL21(DE3) (Novagen) using the T7 promoter system (*32*). All protein expression was performed in M9 minimal media. Uniformly labeled ^{15}N- and $^{15}N/^{13}C$-eotaxin-2 were produced in M9 media supplemented with ^{15}N-ammonium chloride (1 g/L) or ^{15}N-ammonium chloride (1 g/L) and ^{13}C-glucose (2 g/L) (Cambridge Isotope Laboratory, Andover, MA). The cells were grown to an OD_{600} of 0.6−0.9, induced with IPTG (final concentration 1 mM), and harvested 6−8 h after induction. The cell pellets were frozen at −20 °C for at least 12 h, then thawed and resuspended in 10 mL of lysis buffer (20 mM sodium phosphate, 400 mM NaCl, pH 8.0). Hen egg white lysozyme was added to a final concentration of 1 mg/mL, and the cells were subjected to two additional freeze/thaw cycles. The viscous solution was sonicated in three 30 s bursts, with 5 min of incubation on ice between bursts. The lysate was centrifuged at 31000*g*, 4 °C for 30 min, and the supernatant discarded. The inclusion bodies were solubilized in 8 M urea, 100 mM sodium phosphate, 10 mM Tris, 1 mM DTT (denaturing buffer), pH 8.0, by stirring at room temperature for 1 h. The solution was centrifuged at 31000*g*, 25 °C for 30 min, and the supernatant loaded onto a Ni−NTA affinity column (Qiagen, Valencia, CA). The column was washed with denaturing buffer, pH 5.9, and the denatured His_6-tag/eotaxin-2 fusion protein was eluted with denaturing buffer, pH 4.5. Fractions containing fusion protein were pooled and stirred at room temperature with DTT (final concentration 50 mM) overnight. The protein was refolded by dialysis against refolding buffer [50 mM Tris, 0.2% NaN_3, 2.5 mM reduced glutathione (GSH), and 0.5 mM oxidized glutathione (GSSG), pH 8.0] containing 3 M urea for 24 h, refolding buffer with 1 M urea for 24 h, and factor Xa cleavage buffer (50 mM Tris, 100 mM NaCl, 2 mM $CaCl_2$, pH 8.0) for 24 h. The fusion protein was cleaved with factor Xa (New England Biolabs, Beverly, MA; final concentration 10 μg/mg of protein) for 16 h at room temperature. Cleavage was judged to be ~90% by SDS−PAGE analysis. The cleaved protein was loaded onto an HR 10/10 Source 15S cation exchange column (Amersham Pharmacia Biotech, Inc., Piscataway, NJ) and eluted over 1.5 h with a linear gradient of 50 mM−2 M NaCl at 1 mL/min in 20 mM Tris, 2 mM $CaCl_2$, pH 8.0. Eotaxin-2 eluted at ~520 mM NaCl. The protein was dialyzed against H_2O for removal of the salt and concentrated for exchange into the appropriate buffer.

The final yield of eotaxin-2 was ca. 4 mg/L of cell growth with a purity of >95% as judged by SDS−PAGE analysis. N-terminal sequencing and amino acid analysis were performed by the Laboratory for Molecular Structure at Purdue University.

Analytical Ultracentrifugation. Analytical ultracentrifugation was performed on a Beckman Optima XL-I instrument equipped with a model An-60Ti rotor. Eotaxin-2 samples were dissolved at concentrations of 12, 50, and 200 μM in 20 mM sodium acetate, 0.02% NaN_3, pH 4.0. Equilibrium sedimentation data were recorded for each sample at two rotor speeds (35 000 and 45 000 rpm), and each sample was monitored at three wavelengths chosen to maximize the number of data points in the absorbance range 0.1−1.0. The six data sets for each protein concentration were fit simultaneously to the model for a single ideal species using the ORIGIN software provided with the instrument by Beckman.

NMR Spectroscopy. NMR samples consisted of 1−2 mM ^{15}N-labeled or ^{13}C/^{15}N-labeled eotaxin-2 in 20 mM deuterated sodium acetate, 0.02% NaN_3, pH 4.0 buffer. All NMR experiments were collected at 298 K on a Varian Unity-INOVA 500 MHz spectrometer with a triple resonance 3-axis gradient probe. Chemical shifts were referenced to external DSS according to the method of Wishart et al. (*33*). Quadrature detection was achieved using the States-TPPI method (*34*). NOESY experiments were run with a mixing time of 150 ms. Complete details of data collection are available as Supporting Information.

Sequential assignments of backbone resonances were achieved using CBCA(CO)NH (*35*,*36*), HNCACB (*35*−*37*), HBHA(CBCACO)NH (*38*), and 3D ^{15}N TOCSY-HSQC (*39*) data. Side chain assignments were obtained from 3D HCC-TOCSY-CONH (*40*, *41*), CCC-TOCSY-CONH (*40*, *41*), and HCCH-TOCSY (*42*) experiments. Aromatic side chains were assigned using a 3D aromatic HCCH-TOCSY, a 2D (HB)-CB(CGCD)HD (*43*), and NOEs to the β protons. Heteronuclear $\{^1H\}-^{15}N$ NOEs were measured using the pulse sequence of Farrow et al. (*44*).

Geometrical Restraints and Stereospecific Assignments. Distance restraints were obtained from cross-peak volumes in the following NOESY experiments: 3D ^{15}N NOESY-HSQC (*39*), 3D ^{13}C-edited aliphatic NOESY [based on (*45*)], 3D ^{13}C-edited aromatic NOESY, 4D aromatic to methyl ^{13}C HMQC-NOESY-HMQC [based on (*46*)], 4D full aliphatic ^{13}C HMQC-NOESY-HMQC (*46*), and 3D simultaneous ^{13}C/^{15}N-edited NOESY (*45*). Cross-peaks were categorized as strong (1.8−2.8 Å), medium (1.8−3.3 Å), or weak (1.8−5.0 Å) in each data set based on the volumes of intraresidue peaks or cross-peaks corresponding to known distances in secondary structure elements (*47*). To adjust appropriately for center averaging, 1 Å was added to the upper bound of each restraint involving nonstereospecifically assigned methylene protons, 1.5 Å was added for stereospecifically assigned methyl groups, 2.5 Å was added for non stereospecifically assigned methyl groups, and 2 Å was added for aromatic ring protons.

$^3J_{HNH\alpha}$ coupling constants were obtained from a 3D HNHA (*48*, *49*). Backbone ϕ angles were constrained to $-60° \pm 30°$ for $^3J_{HNH\alpha} < 5.5$ Hz, $-120° \pm 60°$ for $^3J_{HNH\alpha} > 7$ Hz (*50*), $-120° \pm 50°$ for $^3J_{HNH\alpha} > 8$ Hz, and $-120° \pm 40°$ for $^3J_{HNH\alpha} > 9$ Hz. In addition, residues with 6 Hz $\leq {}^3J_{HNH\alpha} \leq$ 7 Hz were constrained to be negative if their intraresidue $H_\alpha-H_N$ NOE was weaker than the sequential $H_\alpha-H_N$ NOE (*50*). Side chain χ_1 angles were included for six residues based on analysis of the $^3J_{H\alpha H\beta}$ coupling constants obtained from the HACAHB-COSY (*51*) and inspection of the intraresidue NOE pattern. Gln-46, Tyr-59, Met-60, and Leu-63 all have one $^3J_{H\alpha H\beta}$ strong and one weak, so their χ_1 angles could be constrained to be $-120° \pm 120°$. Ile-38 and Val-56 both have a strong $^3J_{H\alpha H\beta}$ and could be constrained to $-60° \pm 60°$ and $180° \pm 60°$, respectively (*52*).

Stereospecific H_β assignments were made for seven residues (Phe-10, Arg-20, Tyr-24, Phe-39, Trp-55, Met-60, and Leu-63) based on side chain χ_1 conformation and NOE patterns. A 10% ^{13}C-labeled sample of eotaxin-2 was used for the stereospecific assignment of the isopropyl methyl groups of all valines and both leucines according to the method of Neri et al. (*53*).

Slowly exchanging amide protons were identified from a series of 15 min ^{15}N HSQC spectra, with the first spectrum initiated 7 min after dissolving lyophilized fully protonated protein in D_2O buffer. A hydrogen bond restraint was added in the later rounds of structure calculations if the amide proton signal remained after 15 min and if an unambiguous partner was present in at least one-third of the initial structures inspected. Each hydrogen bond was specified as two distance restraints (H_N-O distance of 1.7−2.3 Å and N−O distance of 2.4−3.3 Å).

Structure Calculations. Structure calculations were performed on a Silicon Graphics O2 (R5000 processor) using the hybrid distance geometry-simulated annealing protocol (*54*−*56*) within the program XPLOR (*57*). One hundred structures were generated through substructure embedding and subsequent template fitting to include missing atoms. Each structure was subjected to 1000 steps of high-temperature dynamics at 2000 K for a total of 3 ps, and then cooled to 1000 K over a period of 3 ps (1000 steps at 3 fs/step). Refinement was achieved through a slow-cooling step from 1000 to 100 K (6000 steps at 5 fs/step) and 200 steps of restrained energy minimization. The final family of 20 structures was chosen based on low XPLOR energies, agreement with experimental constraints, and the quality of the structures as determined using the programs AQUA/Procheck (*58*) and What-If (*59*, *60*). The coordinates and input constraints have been deposited in the Protein Data Bank (*61*) (accession codes 1EIH for the ensemble of 20 structures and 1EIG for the energy-minimized average structure).

Receptor Peptide Binding. A linear peptide corresponding to the N-terminal region of CCR3 was synthesized by the Biochemistry Biotechnology Facility at Indiana University Purdue University, Indianapolis, and purified by reversed phase HPLC. The sequence is MTTSLDTVETFGTTSYY-DDVGLLSEKADTRALMAQ; the underlined Ser corresponds to a Cys in the native sequence and was introduced to prevent intermolecular disulfide bond formation. Binding of the peptide to eotaxin-2 was monitored using a series of 20 h ^{15}N HSQC spectra (256 complex t_1 points; 64 transients per fid) on samples containing 94, 92, 89, 85, and 78 μM ^{15}N-labeled eotaxin-2 and increasing amounts (0, 18, 45, 85, and 156 μM, respectively) of peptide. The chemical shifts observed in the presence of the peptide are the population-weighted averages of the chemical shifts of free and bound eotaxin-2. Therefore, the observed chemical shift change ($\Delta\delta_{obs}$) is given by

$$\Delta\delta_{obs} = \Delta\delta_{max}(C/C_{eot}) \quad (1)$$

in which $\Delta\delta_{max}$ is the chemical shift difference between bound and free eotaxin-2, C_{eot} is the total concentration of eotaxin-2, and C is the concentration of bound eotaxin-2, which is given by

$$C = 0.5[(K_d + C_{eot} + C_{pep}) - \sqrt{(K_d + C_{eot} + C_{pep})^2 - 4C_{eot}C_{pep}}] \quad (2)$$

In eq 2, C_{pep} is the total concentration of the peptide and K_d is the dissociation constant of the eotaxin-2−peptide complex. The observed chemical shift changes and the known total peptide and protein concentrations for the 15 residues that undergo the most pronounced concentration-dependent shifts were fitted simultaneously to eqs 1 and 2 to yield a single dissociation constant K_d and a $\Delta\delta_{max}$ for each residue. Fitting was accomplished by χ^2 minimization, and the uncertainty in the K_d was estimated from 500 Monte Carlo simulations.

RESULTS

Protein Expression. A His_6-tag/eotaxin-2 fusion protein was expressed in *E. coli* as insoluble inclusion bodies, which were then solubilized and renatured. Proteolytic removal of the His_6-tag followed by chromatographic purification yielded eotaxin-2 with a native N-terminus, as verified by N-terminal sequencing; previous studies have shown that a native N-terminus is crucial to the activity of other chemokines (*13*−*19*). The molecular weight of the purified eotaxin-2, measured by mass spectrometry, was 8305 amu, which is 473 amu lower than the molecular weight predicted from the amino acid sequence (8778 amu). This suggested the possibility that the five C-terminal amino acids (Ala-Arg-Ala-Val-Ala; combined residue mass 469 amu) had been cleaved during expression or purification. Consistent with this hypothesis, amino acid analysis revealed lower than expected levels of alanine, arginine, and valine, and the five C-terminal residues were also absent from the NMR spectra. Mass spectrometry showed that the His_6-tagged fusion protein had also been truncated at the C-terminus by five residues, indicating that the truncation did not result from nonspecific factor Xa cleavage. Interestingly, eotaxin-2 isolated from a baculovirus/Sf9 insect cell expression system also contains C-terminal truncations corresponding to one, three, and five residues, suggesting that this region is unusually proteolytically sensitive (*23*). The recombinant eotaxin-2 isolated in the current work was active in a calcium flux assay performed with human osteosarcoma cells stably transfected with CCR3 (data not shown) (*62, 63*).

Sedimentation Analysis. Previously, several chemokines have been found to form dimers or higher order oligomers (*10*). To determine whether eotaxin-2 oligomerizes in the buffer used for NMR measurements, equilibrium sedimentation ultracentrifugation was performed (Figure 1). At initial protein concentrations of 12 and 50 μM, the data fit well to a single ideal species with molecular weights of 8269 and 7483 amu, respectively, slightly lower than the calculated monomer molecular weight. At an initial concentration of 200 μM, a fit to a single ideal species yielded an even lower molecular weight (6343 amu), indicating nonideal sedimentation behavior (*64*). This observation is consistent with the high predicted positive charge (+11.7) on eotaxin-2 at the pH of these measurements (pH 4.0). Thus, the sedimentation data showed no evidence of self-association.

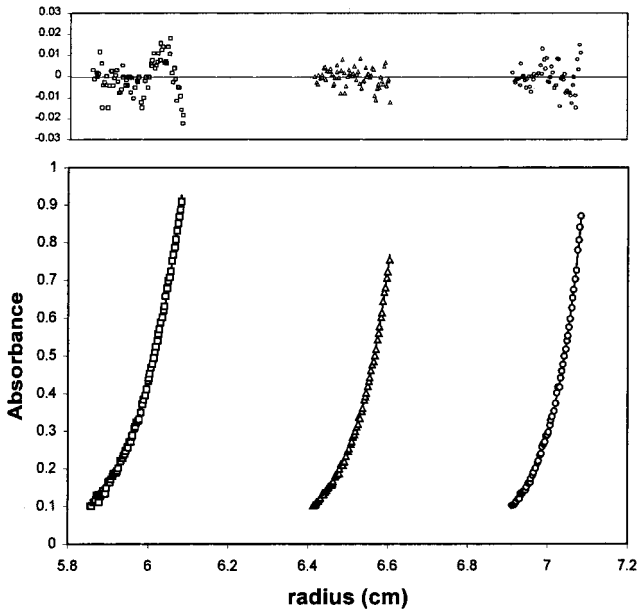

FIGURE 1: Equilibrium sedimentation analysis of eotaxin-2. Sedimentation data (lower panel) are shown for three samples with initial protein concentrations of 12 μM (open circles), 50 μM (open triangles), and 200 μM (open squares). These data were collected at 25 °C and a rotor speed of 45 000 rpm, and absorbances were detected at 234, 266, and 299 nm, respectively. The solid lines in the lower panel and the residuals shown in the upper panel were obtained by globally fitting the six data sets acquired at each protein concentration (see Materials and Methods) to an equation describing a single, ideal species.

Assignments and Secondary Structure. Complete backbone and almost complete side chain ^1H, ^{15}N, and ^{13}C resonance assignments were obtained for eotaxin-2 using the experiments described under Materials and Methods; a list of assignments is available as Supporting Information. Long-range NOEs were assigned using several 3D and 4D NOESY experiments. 4D experiments were required due to significant spectral overlap in the methyl and aromatic regions of the spectrum. For example, in the hydrophobic core, there were three methyl proton resonances at 0.96 ppm, three at 1.09 ppm, and five at ~0.90 ppm, five aromatic proton resonances at 6.75 ppm and three at 7.37 ppm.

A summary of the secondary structural information of eotaxin-2 is shown in Figure 2. Based on NOE patterns, coupling constants, and chemical shift indices, eotaxin-2 is deduced to possess a single turn of helix, three β-strands, and a C-terminal α-helix, consistent with previous chemokine structures (*10*). A total of 18 amide protons show protection from deuterium exchange 15 min after dissolution. This is similar to the hydrogen exchange pattern of eotaxin, in which 17 amide protons persisted 10 min after dissolution (*65*). In addition, the amides of either or both Gln-25 and Thr-40 in eotaxin-2 are protected; this assignment remains ambiguous because the amide signals are overlapped.

Three-Dimensional Structures. The input restraints used for the final round of structure calculations are listed in Table 1. These consist of 854 distance, 48 dihedral angle, and 12 × 2 hydrogen bond restraints, a total of 15.4 restraints per

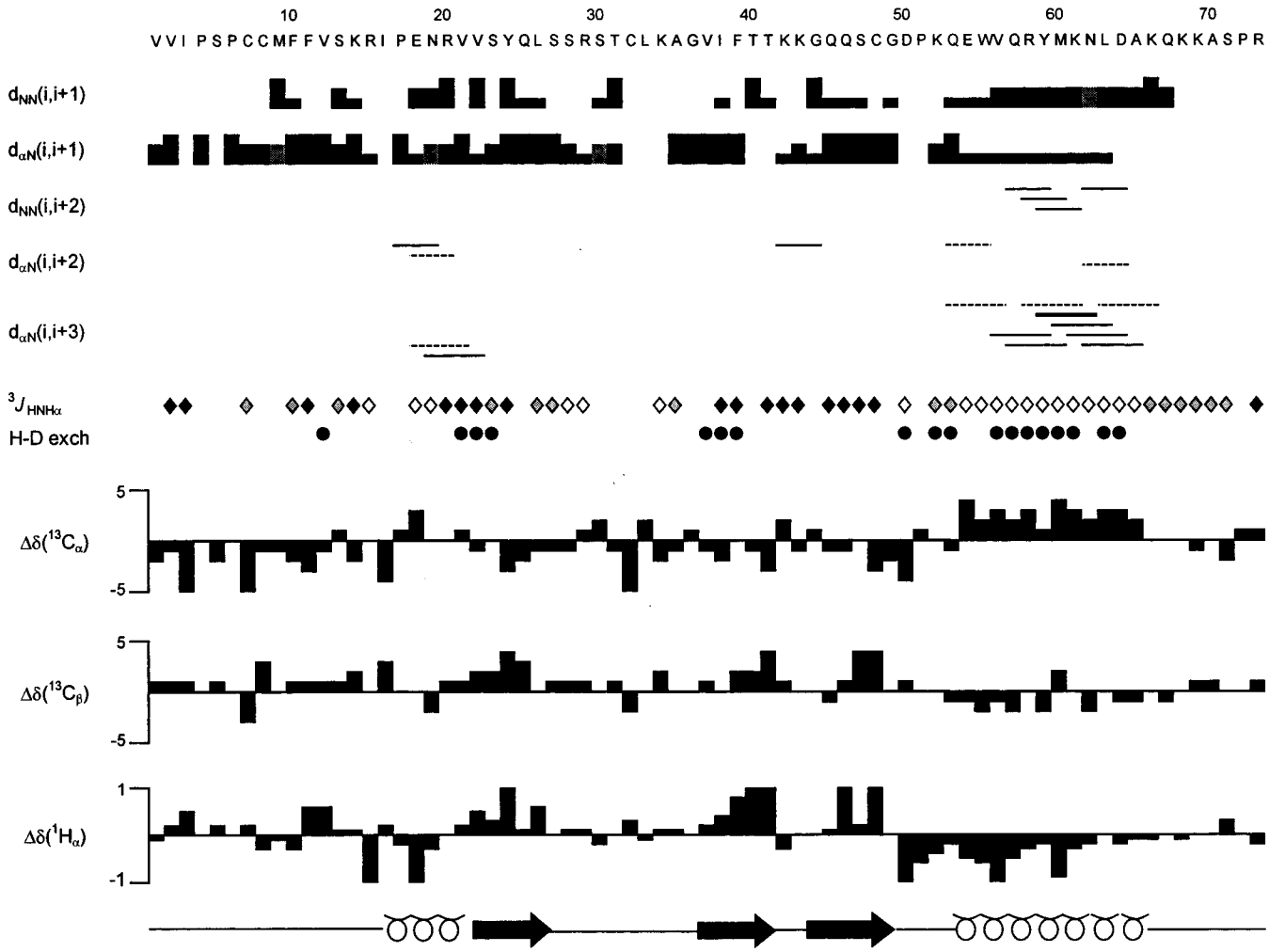

FIGURE 2: Summary of secondary structure information for eotaxin-2. The amino acid sequence and numbering are shown at the top. Sequential N−N and α-N NOEs are indicated by black bars; the thickness of the bar represents the strength of the observed NOE. The presence of medium-range N−N and α-N NOEs is indicated by solid lines. Gray bars and dashed lines represent ambiguous assignments. $^3J_{HNH\alpha}$ coupling constants are represented by diamonds corresponding to values of <6 Hz (white), 6−8 Hz (gray), and >8 Hz (black). Residues whose amide protons show protection from exchange with solvent are indicated with filled circles. The chemical shift indices shown for C_α, C_β, and H_α were calculated according to the method of Wishart and Sykes (*83, 84*). The locations of the secondary structure elements identified in the calculated family of structures are shown at the bottom.

Table 1: Summary of Input Restraints

distance restraints (total 854)	
intraresidue ($i - j = 0$)	367
sequential ($\|i - j\| = 1$)	197
short range ($\|i - j\| \leq 4$)	95
long range ($\|i - j\| > 4$)	195
dihedral restraints (total 48)	
ϕ	42
χ_1	6
hydrogen bonds	12 × 2
total restraints	926
total restraints per residue	12.7
total restraints per ordered residue (7−66)	15.4

well-ordered residue (Figure 3A). Structure calculations were performed for a monomeric species, which is well supported by the following evidence: (1) sedimentation data are consistent with the protein being monomeric up to concentrations greater than 200 μM; (2) ^{15}N HSQC spectra collected using 1 mM samples at various pH, ionic strength, and temperature conditions did not exhibit dimer peaks similar to those observed for eotaxin (*65*) and did not show any significant line broadening; (3) all of the observed NOEs were consistent with the calculated monomer structure (Table 2); (4) no NOEs could be identified indicating either of the two dimerization modes previously described for chemokines (*10*); and (5) the N-terminal region of eotaxin-2 exhibits low heteronuclear NOEs (Figure 3D) and minimal protection from amide proton exchange, suggesting that it does not participate in a well-ordered dimer interface.

The quality of the final family of 20 structures is good, with no NOE violations greater than 0.3 Å and no dihedral angle violations greater than 1.5°, small deviations from ideal geometry, and approximately 99% of the well-ordered $\phi-\varphi$ angle pairs in the most favored regions of Ramachandran space (Table 2). The rmsd values for the final 20 structures measured against the average structure are shown in Figure 3B,C. Over the whole protein, the average rmsd is 1.36 Å for the backbone (C_α, N, C′) and 2.00 Å for all heavy (non-hydrogen) atoms. If the rmsd is calculated over only the well-ordered residues 7−66 (see below), the rmsd values decrease dramatically to 0.52 and 1.13 Å, respectively. Removal of the less well-defined part of the 30s loop (residues 28−34; see below) further decreases these values to 0.41 and 0.92 Å, respectively.

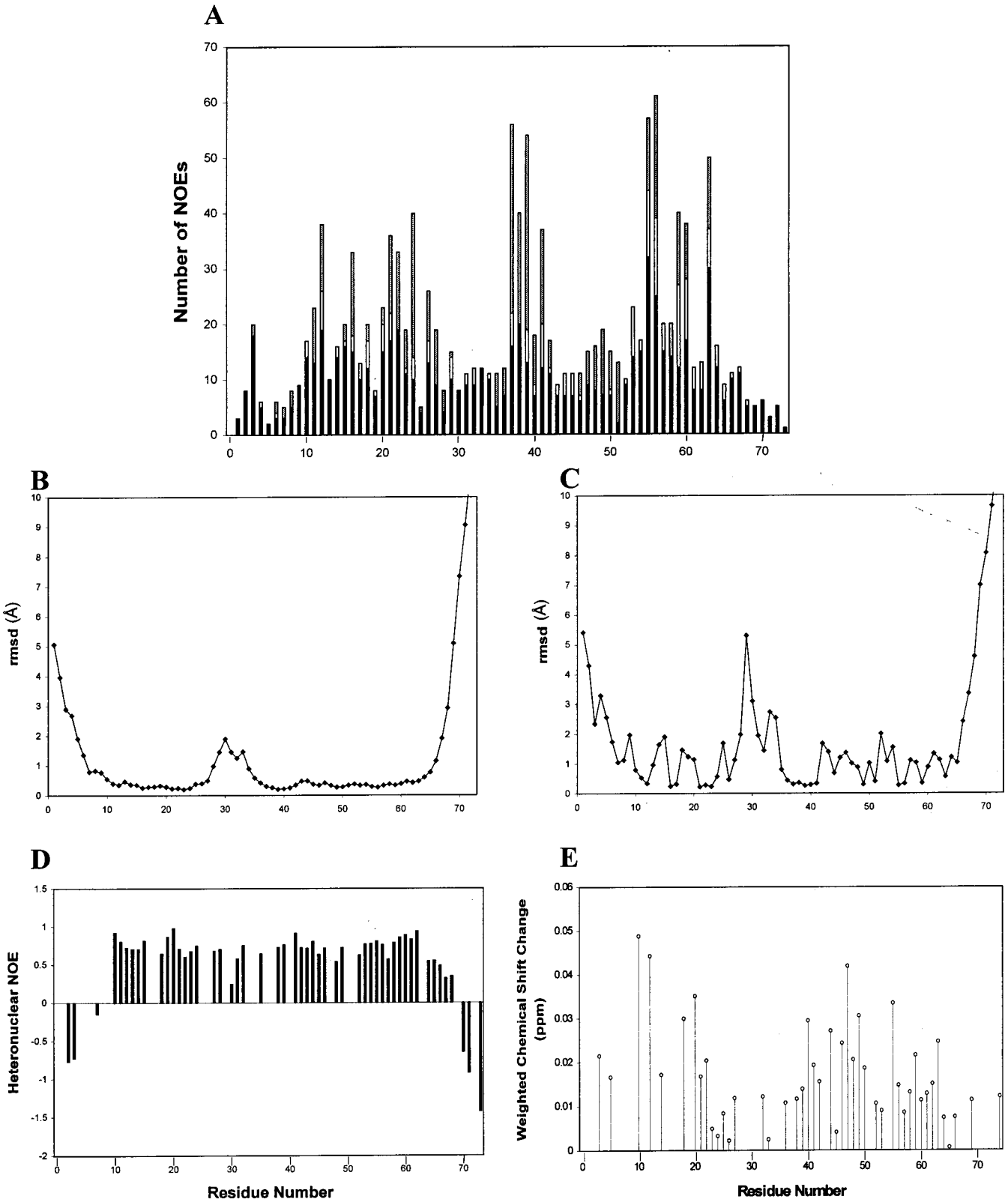

FIGURE 3: (A) Number of NOE restraints per residue. NOEs between residues *i* and *j* are categorized (from bottom to top) as intraresidue ($i = j$, solid bars), sequential ($|i - j| = 1$, horizontal lines), medium range ($1 < |i - j| = 4$, open bars), or long range ($|i - j| > 4$, gray bars). (B and C) Average backbone (B) and heavy atom (C) rmsd values for the family of 20 structures relative to the average structure. (D) Heteronuclear $\{^1H\}-^{15}N$ NOEs for each backbone NH group. (E) Weighted chemical shift changes of each backbone amide group upon receptor peptide binding. Shifts were measured for a sample containing 78 μM protein and 156 μM peptide; under these conditions, the protein is 85% bound. Weighted chemical shift changes were calculated by addition of the chemical shift change of the amide protein to one-fifth of the chemical shift change of the amide nitrogen (*85*).

The family of 20 structures and the energy-minimized average structure of eotaxin-2 are shown in Figure 4. The structure is consistent with the other chemokine structures that have been determined (*10*). The N-terminal region

Table 2: Results of Calculations

	<eotaxin-2>[a]	eotaxin-2_min[b]
rmsd from ideal geometry		
bonds (Å)	0.0025 ± 0.0001	0.0018
angles (deg)	0.60 ± 0.01	0.55
impropers (deg)	0.47 ± 0.02	0.43
rmsd from exptl restraints		
distance (Å)	0.024 ± 0.001	0.018
dihedral angle (deg)	0.23 ± 0.04	0.226
NOE violations per structure		
>0.3 Å	0	0
>0.2 Å	0.35	0
>0.15 Å	2.65	0
dihedral violations per structure		
>1.5°	0	0
>1°	0.8	0
>0.5°	2.9	3
XPLOR energies (kcal mol^{-1})		
overall	187.8 ± 5.1	147.8
bond lengths (Å)	7.7 ± 0.6	4.1
bond angles (deg)	119.1 ± 4.8	98.4
improper (deg)	20.1 ± 1.4	17.2
van der Waals (deg)	14.5 ± 4.1	13.4
NOE	26.2 ± 2.8	14.6
dihedral (deg)	0.16 ± 0.05	0.14
Ramachandran analysis		
(residues 7−66) (%)		
most favored regions	72.3	72.7
additional allowed regions	26.3	27.3
generously allowed regions	1.4	0.0
disallowed regions	0.1	0.0
rmsd from mean structure (Å)		
all residues (backbone/ heavy atoms)	1.36/2.00	
residues 7−66	0.52/1.13	
residues 7−27, 35−66	0.41/0.92	

[a] Family of 20 structures. [b] Average minimized structure.

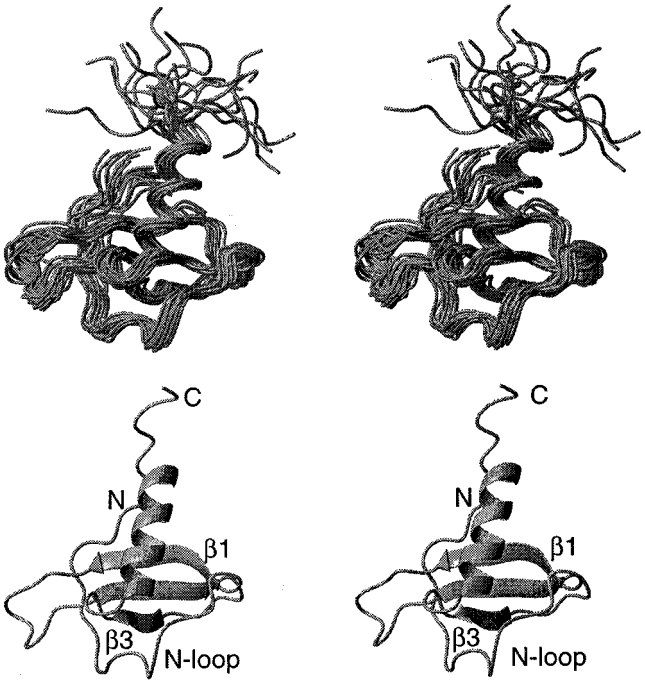

FIGURE 4: Stereo representations of the family of 20 structures calculated for eotaxin-2 (top) and the energy-minimized average structure (bottom). This figure was generated using the program Molmol (*86*).

(residues 1−6), preceding the CC motif, is largely disordered with rmsd values of 1.5−5 Å and negative heteronuclear NOEs (Figure 3D). However, there are four long-range NOEs indicating that residues Ile-3 and Pro-6 spend a significant proportion of time in close proximity to residues Tyr-24 and Ile-38 in the β-sheet. The N-loop region (residues 9−16) extends from the CC motif to a helical turn (residues 17−20) and contains non-hydrogen-bonded bends at residues Met-9/Phe-10 and Ser-13/Lys-14. The helical turn appears to be intermediate between an α-turn and a 3_{10}-turn. In all 20 structures, the carbonyl oxygen of Pro-17 has a bifurcated hydrogen bond to the amide hydrogens of residues Asp-20 (i,i+3) and Val-21 (i,i+4), although neither of these hydrogen bonds was specified as a restraint in structure calculations. This turn, when present in other chemokines, is usually 3_{10} in nature (*10*).

The helical turn is followed by the first strand (residues 22−26) of a three-stranded antiparallel β-meander. The second and third β-strands comprise residues 37−41 and residues 44−49, respectively. Strand β1 contains a classic β-bulge involving residues Val-22, Ser-23, and Thr-40 [positions 1, 2, and X, respectively (*66*)], and strand β3 contains a G1 β-bulge involving residues Gly-44, Gln-45, and Thr-41 [positions 1, 2, and X, respectively (*66*)]. The 7 central residues (28−34) of the 10-residue loop connecting strands β1 and β2 (the 30s loop) are not well-defined by the experimental data, whereas strands β2 and β3 are connected by an ordered type I/III turn. Strand β3 is followed by a well-defined type III turn leading into a regular α-helix that extends from residues 54 to 66. The C-terminus (residues 67−73) shows no long-range NOEs to the rest of the protein and is completely disordered, with large rmsd values and negative heteronuclear NOEs (Figure 3).

The tertiary structure of eotaxin-2 involves extensive hydrophobic interactions between the α-helix and the β-sheet. The helix lies across one face of the β-sheet, forming an angle of ∼75° with the direction of the β-strands (Figure 4). The hydrophobic side chains of residues Tyr-24 and Leu-26 (in strand β1), Val-37 and Phe-39 (in strand β2), and Pro-51 (in the β3−α-turn) cluster together with hydrophobic residues Trp-55, Val-56, Tyr-59, Met-60, and Leu-63 from one side of the amphipathic α-helix. In addition, residues Phe-11, Val-12, and Ile-16 (in the N-loop) and Val-21 (immediately following the helical turn) make hydrophobic contacts with each other and with Phe-39, Pro-51, Trp-55, and Tyr-59 in the core.

In the N-terminal region of the sequence, residues Ser-5 to Met-9 extend across the face of the β-sheet opposite from the α-helix, forming an angle of ∼90° with the direction of the β-strands (Figure 4). The N-terminal region is tethered to this face of the β-sheet by the two conserved disulfide bonds. The first disulfide, between Cys-7 and Cys-32 (in the 30s loop) is poorly defined, whereas the second disulfide, between Cys-8 and Cys-48 (in strand β3), is better defined and is consistent with the left-handed spiral seen in most other chemokine structures (*10*). The interface between the N-terminal region and the β-sheet appears to be further stabilized by hydrophobic contacts between the side chains of Ile-3, Pro-6, Cys-8, Gln-25, Ile-38, and Cys-48.

The calculated structures are in good agreement with the observed hydrogen exchange data. Of the 18 amide protons that are resistant to exchange, 12 were restrained in hydrogen bonds in the structure calculations. Ten of these correspond to the β-sheet and α-helix regions. A hydrogen bond from

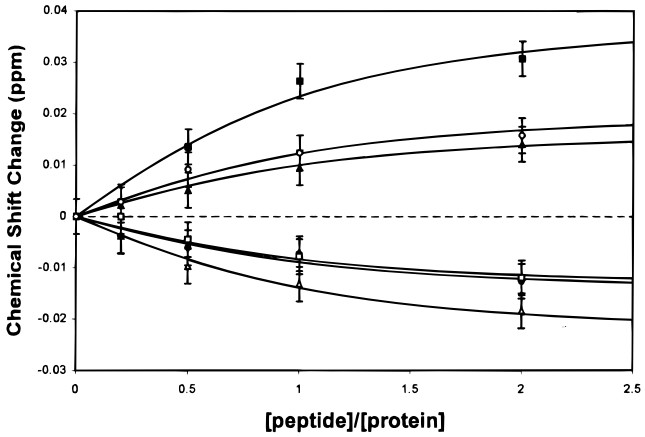

FIGURE 5: Example of binding isotherms obtained upon titration of eotaxin-2 with the N-terminal CCR3-derived peptide. The chemical shift change is plotted as a function of peptide/protein ratio for the amide protons of Phe-10 (filled squares), Val-12 (open triangles), Glu-18 (filled circles), Cys-32 (open squares), Tyr-59 (filled triangles), and Leu-63 (open circles). Error bars correspond to the ^{1}H digital resolution of the HSQC spectra. The solid lines were obtained by globally fitting the data for 15 shifted residues (see Materials and Methods).

the amide of Val-12 to the carbonyl of Cys-48 tethers the N-loop region to strand β3. The remaining restraint is from Gln-53 to Asp-50 in the β3−α-turn. Among the six protected amide protons that do not have hydrogen bond restraints associated with them, one (Val-21) is hydrogen bonded in the helical turn (see above), and three (Ser-23, Asp-50, and Val-56) are buried but not involved in hydrogen bonds. The amide of Lys-52 is hydrogen-bonded across the β3−α-turn to one of the side chain oxygens of Asp-50 in 13 of the 20 structures. Finally, the amide of Gln-57 is at the N-terminus of the α-helix and may be transiently hydrogen bonded to the carbonyl of Gln-53 (this distance is 2.87 Å in the average minimized structure).

Receptor Peptide Binding. Previous studies have shown that peptides corresponding to the N-terminal regions of the IL-8 receptor (CXCR1) and the fractalkine receptor (CX_3-CR1) bind to the chemokines IL-8 and fractalkine, respectively, with low affinity ($K_d = 170 \pm 50$ μM for IL-8; K_d in μM−mM range for fractalkine) (*11*, *20*, *67*). To determine whether this interaction also occurs for the CC chemokine eotaxin-2 and to identify the region of eotaxin-2 that interacts with the N-terminal region of the receptor, we have monitored the HSQC spectrum of eotaxin-2 in the presence of increasing concentrations of an N-terminal receptor peptide [CCR3(1−35)]. Upon addition of peptide, several backbone amide resonances undergo subtle but concentration-dependent chemical shift changes. The magnitudes of the observed changes are plotted in Figure 3E, and binding isotherms for six of the most strongly affected proton resonances are shown in Figure 5. Simultaneous fitting of the binding isotherms, assuming 1:1 stoichiometry, yielded a consensus dissociation constant of 45 μM (90% confidence range 3−148 μM). In addition to the observed shifts, eight amide resonances (Ser-5, Cys-7, Cys-8, Phe-11, Ile-16, Lys-34, Ala-35, and Val-37) underwent noticeable changes in line shape (broadening and/or distortion) in response to addition of peptide, and an additional two peaks (Arg-15 and Glu-54) disappeared from the spectrum, possibly due to extreme broadening. The effects of peptide binding on 15 residues could not be measured because these NH groups exchange too rapidly with water at the pH of this study (pH 6.5).

The positions of the NH groups that undergo concentration-dependent chemical shift changes or line broadening upon peptide binding are shown in Figure 6A. These residues are distributed throughout the N-terminus, N-loop, helical turn, β2−β3 hairpin, and α-helix. The surface characteristics of this region and the possible location of the peptide binding site are discussed below.

DISCUSSION

Receptor Peptide Binding Site. Many of the residues that are affected by receptor peptide binding are clustered together in the N-loop or the β2−β3 hairpin regions of the eotaxin-2 structure. A space-filling representation of eotaxin-2 highlighting the interface between these two regions is presented in Figure 6B. A shallow (∼5−6 Å deep) extended groove is located on the front face of the structure. The left-hand edge of this groove is defined by the side chains of residues Cys-7 and Cys-8 (the CC motif) and residues Met-9, Phe-10, Ser-13, Lys-14, and Arg-15 from the N-loop, whereas the right-hand edge of the groove consists of residues Pro-17 and Arg-20 from the helical turn, Thr-41 from the β2−β3 turn, and Gln-45 and Gln-46 from the beginning of the β3-strand. While many of the residues defining the edges of this channel are charged or polar, the floor of the groove is formed predominantly by hydrophobic side chains including Val-12 and Ile-16 from the N-loop, Trp-55 from the α-helix, Cys-48 from the β3-strand, and Ile-38 from the β2-strand. The side chain of Ser-47 also contributes to the base of the groove. The 3D structure of this region is maintained by the clustering of hydrophobic side chains as well as by the two conserved disulfide bonds and a single hydrogen bond between the amide of Val-12 and the carbonyl of Cys-48. This groove is referred to below as the N-loop/β3 groove.

The N-loop/β3 groove is also present in the structures of other chemokines and has been proposed to be the binding site for the N-terminal region of chemokine receptors. This assertion is supported by the evidence that: (1) peptide binding studies similar to those described here indicate chemical shift changes in this region of the structure (*11*, *67*); (2) the solution structure of a complex between IL-8 and an N-terminal peptide derived from CXCR1 shows the peptide lying in an extended conformation in this groove (*20*); and (3) chemokine mutational analysis has identified N-loop side chains as making substantial energetic contributions to receptor binding (*12*, *17*).

The current peptide binding results are consistent with the proposal that the N-terminal peptide from CCR3 lies in the N-loop/β3 groove of eotaxin-2. In particular, the NH groups of almost all residues in the N-loop and helical turn are either shifted or broadened upon peptide binding as are those of several residues in the β2−β3 hairpin. All of the shifted residues in these structural elements either contribute directly to the definition of the groove or are adjacent in the primary sequence to the residues that line the groove. It is important to note that chemical shift changes could potentially result either from direct interactions with the peptide or from chemokine structural changes induced by peptide binding. Thus, the chemical shift perturbation data presented here would be consistent with binding of the receptor peptide to

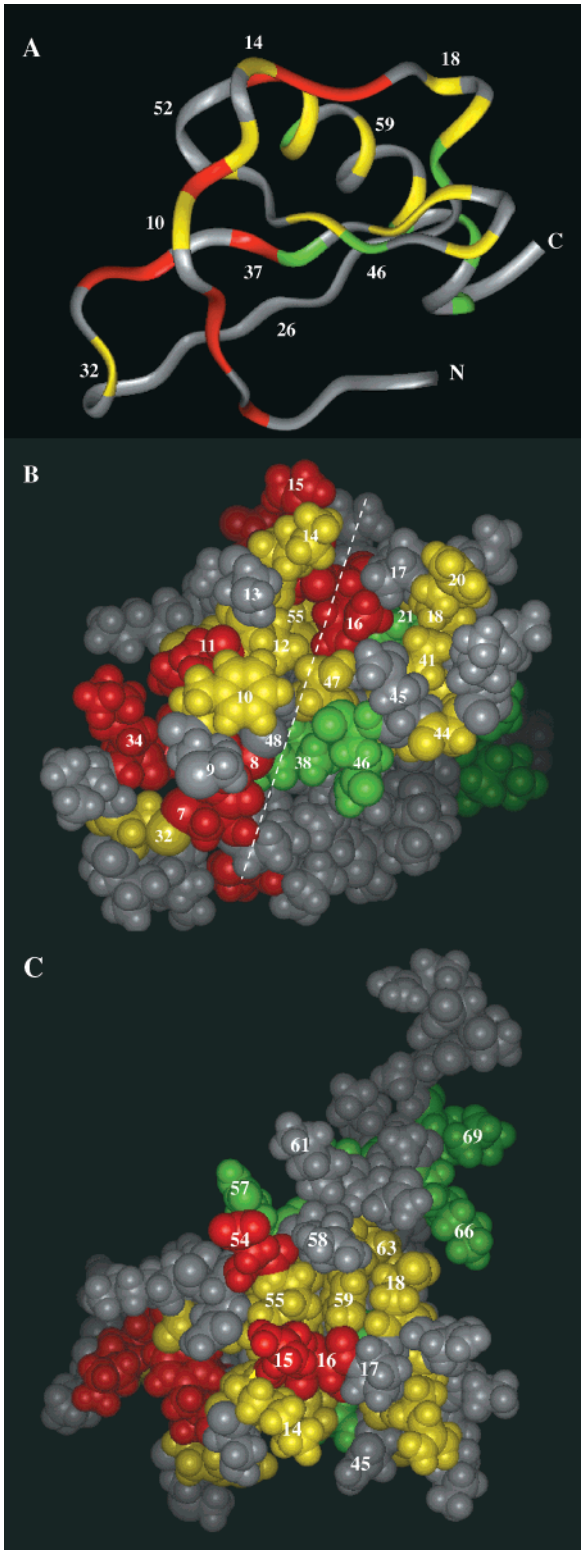

FIGURE 6: Average minimized structure of eotaxin-2 color-coded to indicate the residues affected by receptor peptide binding. (A) Ribbon and (B) space-filling representations oriented with the N-loop/β3 groove on the front face of the structure, as indicated by the dashed line. (C) A space-filling representation rotated 90° around the horizontal axis relative to the views shown in (A) and (B). The top of the N-loop/β3 groove is now at the bottom of the structure, and the proposed secondary binding surfaces are visible (see text for details). Residues whose amide protons undergo a concentration-dependent ^{1}H chemical shift change $\geq$0.0102 ppm (3 points) or $<$0.012 ppm (3 points) are yellow and green, respectively, and those whose line shapes changed (see text) are red.

different regions of the eotaxin-2 surface if such binding gives rise to a structural rearrangement of the N-loop/β3 groove region. However, the large number of chemical shift changes observed for residues in the N-loop and β2$-$$\beta$3 hairpin regions is strongly suggestive that the N-loop/β3 groove is itself the peptide binding site.

In addition to the spectral changes observed for residues lining the N-loop/β3 groove, a number of residues that do not contribute to this groove are also affected by peptide binding, including several from the N-terminal region and several from the α-helix. The peak distortion observed in the N-terminus, including both Cys-7 and Cys-8, can be readily explained by proposing that the receptor peptide extends from the bottom end of the N-loop/β3 groove (as shown in Figure 6B) making transient contacts with the N-terminus of the chemokine. In this regard, it is noteworthy that NMR relaxation studies of eotaxin, vMIP-II, and fractalkine have provided evidence for a microsecond$-$millisecond time scale conformational rearrangement in the vicinity of the two disulfide bonds (*67*$-$*70*). It is possible that peptide binding accentuates or modifies the time scale of this conformational fluctuation of the chemokine, resulting in increased line broadening. Alternatively, the observed broadening may result either from sensitivity of the chemokine to conformational fluctuations of the receptor peptide or from intermediate time scale association$-$dissociation kinetics for the chemokine$-$peptide complex.

The spectral changes observed in the α-helical region can also be explained by proposing an extension of the receptor peptide binding site, in this case from the top end of the N-loop/β3 groove (as depicted in Figure 6B). Figure 6C shows a space-filling representation of the eotaxin-2 structure that is rotated 90° relative to that in Figure 6B; the top of the N-loop/β3 groove (as seen in Figure 6B) is now located at the bottom of Figure 6C. This view indicates that, if the peptide were to continue winding around the chemokine surface, bending to the left at the top of the N-loop/β3 groove, it would come into contact with the side chains of Trp-55 and Tyr-59 and pass between the side chains of Arg-15, Glu-54, and Gln-57 (on the left) and Arg-58 and Lys-61 (on the right). On the other hand, if the peptide were to turn to the right at the top of the N-loop/β3 groove, it could then extend approximately parallel to the helix axis, coming into contact with Tyr-59, Leu-63, and Lys-66 from the α-helix and Glu-18 from the N-loop. The current data do not strongly favor one of these possible binding surfaces over the other. The subtle chemical shift change observed for Gln-57 and the disappearance of Glu-54 from the spectrum appear to favor the first possibility. However, the chemical shift changes for Leu-63, Lys-66, Lys-69, and Glu-18 offer support for the second binding surface. It is possible that transient contacts are formed with both of these surfaces. Alternatively, only one of these surfaces may participate in direct interactions with the receptor peptide, and the changes observed in the other region could then result from subtle structural changes of the helix.

Structural Comparison of Eotaxin-2 and Other Chemokines. Eotaxin-2 and the other members of the eotaxin subgroup of CC chemokines have 34$-$38% sequence identity to each other and 31$-$65% sequence identity to the monocyte chemoattractant proteins (MCP-1, MCP-2, MCP-3, and MCP-4). However, the eotaxin subgroup chemokines are all

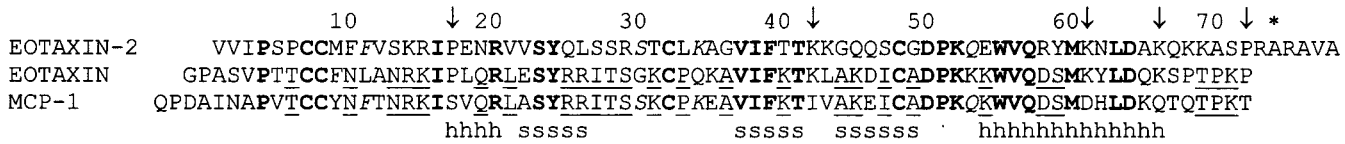

FIGURE 7: Sequence alignment of eotaxin-2, eotaxin, and MCP-1 indicating those residues that are conserved between all three chemokines (boldface), identical between only eotaxin-2 and eotaxin (arrows), identical between only eotaxin-2 and MCP-1 (italics), and identical between only eotaxin and MCP-1 (underlined). The numbering is according to the sequence of eotaxin-2. The asterisk indicates the first of the five residues missing in the truncated protein. The positions of helical (h) and β-strand (s) regions are indicated at the bottom.

specific for the receptor CCR3, whereas the MCP subgroup chemokines either do not activate CCR3 (in the case of MCP-1) or activate other receptors in addition to CCR3. Among these two CC chemokine subgroups, 3D structures have been reported for eotaxin (*65*), MCP-1 (*71, 72*), and MCP-3 (*73, 74*). In combination with these previous structures, the current structure and peptide binding data for eotaxin-2 offer the opportunity to explore the structural features of the eotaxin subgroup chemokines that may be responsible for CCR3 specificity. To this end, we present below a detailed comparison of the structures of eotaxin-2, eotaxin, and MCP-1. We identify several features that are similar in eotaxin and eotaxin-2 but differ in MCP-1; these features are possible specificity determinants for receptor binding.

The sequences of eotaxin-2, eotaxin, and MCP-1 are aligned in Figure 7; note that the residue numbers are 2 higher for eotaxin and 4 higher for MCP-1, in comparison to eotaxin-2, as a result of the different lengths of the N-termini. There are only five residues that are identical between eotaxin-2 and eotaxin but different in MCP-1. One of these (Pro-17 in eotaxin-2; Ser in MCP-1) contributes to the N-loop/β3 binding groove and may therefore be involved directly in receptor discrimination. Another two (Lys-61 and Lys-66 in eotaxin-2; Asp and Gln, respectively, in MCP-1) are located on the surface of the α-helix, one in each of the two locations proposed above as secondary binding sites for the N-terminal receptor peptide. The Lys-61 to Asp charge reversal mutation is a particularly attractive candidate for controlling receptor specificity. The remaining two positions, Lys-42 in eotaxin-2 (Ile in MCP-1) and Pro-72 in eotaxin-2 (Thr in MCP-1), are distant from the binding site proposed above and unlikely to be involved directly in receptor discrimination.

The energy-minimized average structures of eotaxin-2, eotaxin, and MCP-1 are very similar. The average pairwise rmsd for well-defined backbone atoms (corresponding to residues 7−66 of eotaxin-2) is 1.64 Å between eotaxin-2 and eotaxin, 1.71 Å between eotaxin-2 and MCP-1, and 1.36 Å between eotaxin and MCP-1. The angle of the α-helix relative to the β-sheet is almost identical for all three chemokines, consistent with the strong conservation of hydrophobic core residues. Several regions of the structure exhibit subtle conformational differences. The C-terminus of the β1-strand and the N-terminus of the β2-strand are one residue shorter in eotaxin-2 relative to the other two chemokines, thus increasing the length of the relatively disordered 30s loop in eotaxin-2. There are also subtle differences between these three chemokines in the conformation of the classic β-bulge (in β1), the hydrogen bonding patterns in the β2−β3 reverse turn and G1 β-bulge (in β3), and the backbone conformation of the N-loop. However, none of these changes results in any systematic structural difference between the eotaxin subgroup chemokines and MCP-1 that could account for the difference in receptor specificity. In contrast, the N-terminus of the α-helix, which does contribute to the proposed binding surface, extends by an additional one residue in eotaxin-2 and two residues in eotaxin compared with MCP-1. Conformational differences in this region could potentially affect the ability of the receptor peptide to interact with the base of the α-helix.

In contrast to the subtle differences in secondary and tertiary structure, there are more dramatic differences in the quaternary structures of eotaxin-2, eotaxin, and MCP-1. Under the conditions used for solution structure determination, MCP-1 is a dimer [$K_d = 33 \pm 18$ μM, (*75*)], eotaxin exhibits a monomer−dimer equilibrium [$K_d \sim 8.5-18$ mM, (*65*)], and eotaxin-2 is monomeric. Dimerization of MCP-1 (*71*), and apparently also of eotaxin (*65*), occurs by antiparallel pairing of the N-terminal/N-loop regions of the two monomers. Thus, the differences in dimerization propensity may be attributed to the different lengths of the N-termini (*76*) and/or sequence substitutions in this region. Although these differences in quaternary structure raise the possibility that receptor specificity could be related in some way to quaternary structure, there is significant evidence to suggest that the active form of chemokines is the monomer. In particular, chemokine oligomerization is sufficiently weak that chemokines would be expected to be monomeric at their physiological concentrations and chemokines that have been covalently modified to prevent dimerization retain activity (*77*−*79*). Nevertheless, Hoogewerf et al. (*80*) have presented evidence that chemokine oligomerization is enhanced by cell surface glycosaminoglycans, and the dimerization of truncated variants of MIP-1β is increased under physiological solution conditions relative to those typically used for structural studies (*81*). Thus, the relevance of chemokine oligomerization to activity remains somewhat controversial.

Given that the differences in monomer conformation are very subtle and the relevance of quaternary structure is unclear, we further investigated the possibility that the modest tertiary structural differences lead to a more pronounced difference between the surface characteristics of the eotaxin subgroup chemokines in comparison to MCP-1. Figure 8A shows a surface representation of eotaxin-2 color-coded by hydrophobicity. The peptide binding groove discussed above appears as a strip of hydrophobic surface extending diagonally from the top right to the bottom left regions of the structure with the top of the groove bordered by hydrophilic residues. These features are very similar in eotaxin and MCP-1 (not shown). Greater variation of hydrophobicity occurs for the protein surfaces adjacent to the lower half of the structure, partly due to the N-loop sequence differences (the Met-9-Phe-10 sequence in eotaxin-2 corresponds to Phe-Asn in eotaxin, and Tyr-Asn in MCP-1). However, there is

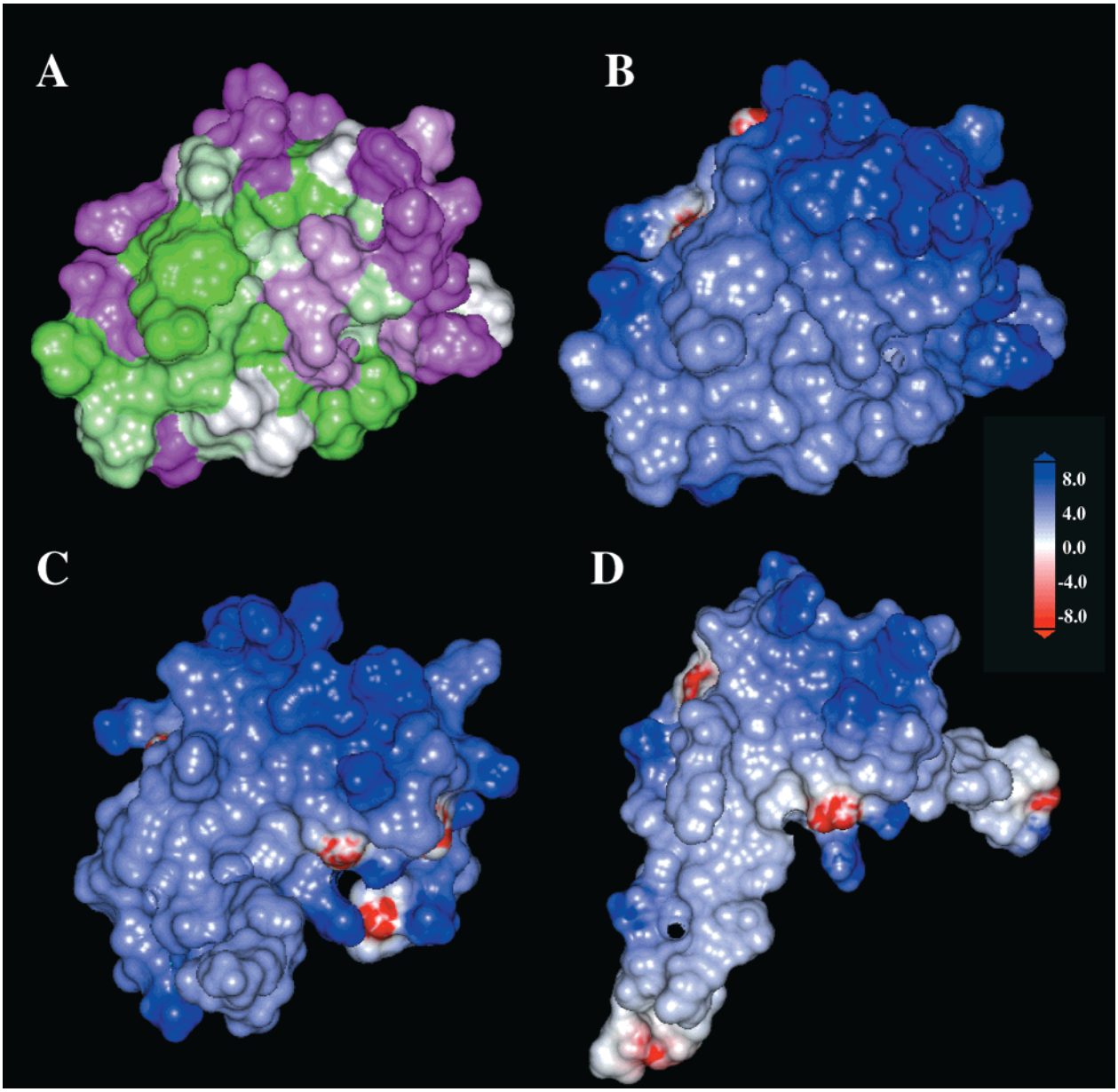

FIGURE 8: Surface representations of eotaxin-2, eotaxin, and MCP-1 in the same orientation as Figure 6A,B. The MCP-1 model shown is one monomer from the dimeric structure. The difference in the shapes of the proteins arises from the conformations of the N- and C-termini in the average minimized structures. (A) Eotaxin-2 color-coded according to hydrophobicity; hydrophobic regions are green, and polar regions are magenta. (B) Eotaxin-2, (C) eotaxin, and (D) MCP-1 color-coded according to electrostatic potential; positive regions are blue, and negative regions are red. Electrostatic potentials, hydrophobicity, and surface shapes were calculated using the programs DelPhi and Insight II (Molecular Simulations Inc., San Diego, CA).

no convincing systematic difference between the eotaxin group chemokines and MCP-1. It is noteworthy that the other faces of all three structures are significantly more hydrophilic than the face on which the N-loop/β3 groove is located.

Figure 8B−D shows surface representations of the eotaxin-2, eotaxin, and MCP-1 monomers color-coded according to electrostatic potential. The shape of the MCP-1 surface in this orientation differs from those of eotaxin and eotaxin-2 owing to the conformations of the N- and C-termini in the average minimized structures. Although all three molecules exhibit predominantly positive potentials, the electrostatic potentials of eotaxin-2 and eotaxin are clearly higher than that of MCP-1 in the vicinity of the N-loop/β3-groove; a similar trend is observed for the other regions of the surface (not shown). This dramatic difference is initially surprising because the isoelectric points (calculated from sequence) for these three chemokines differ relatively slightly (10.0 for eotaxin-2; 9.9 for eotaxin; and 9.4 for MCP-1). Presumably, the differences in the surface electrostatic potential are accentuated by the relative orientations of polar groups on the surfaces of the three chemokines. It is also noteworthy that, despite the similarity in the locations of hydrophobic residues inside the putative receptor binding grooves of the three chemokines (see above), the electrostatic potential inside the groove is strongly positive for eotaxin-2 and eotaxin but only weakly positive for MCP-1. The occurrence of positive potential inside a hydrophobic groove is initially surprising but may be rationalized by the positions of several positively charged residues lining the edges of the groove. This situation is somewhat analogous to the high negative electrostatic potential in the minor groove of B-DNA, which is caused by the additive effects of the backbone phosphate

groups on the outside edge of the groove (*82*). The systematic difference between the electrostatic potentials of the eotaxin subgroup chemokines and MCP-1 (especially in the putative binding groove) provides an attractive possible mechanism for differentiating between the receptors CCR3 and CCR2.

Differences in the electrostatic potentials are particularly pronounced on the α-helix faces of these three chemokines (not shown). Specifically, the region at the base of the helix, corresponding to the short channel formed by the side chains of Arg-15, Glu-54, Gln-57, Arg-58, and Lys-61, is extremely electropositive in both eotaxin-2 and eotaxin but only very slightly positive in MCP-1. This difference may result from the substitution of Lys-61 in eotaxin-2 (Lys-63 in eotaxin) by an Asp in MCP-1. The only other charge variation in this region is the replacement of Arg-58 by Asp in both eotaxin and MCP-1, although this difference does not correlate with the differences in electrostatic potential. The alternative surface suggested above for the extension of the receptor peptide parallel to the α-helix also shows a higher positive potential for both eotaxin-2 and eotaxin relative to MCP-1. This difference appears to be dominated by the substitution of Lys-66 in eotaxin-2 (Lys-68 in eotaxin) by a Gln in MCP-1.

Concluding Remarks. The solution structure of eotaxin-2 and the receptor peptide binding studies presented here support the proposal that the N-terminal region of the CCR3 receptor binds into an extended, shallow cleft in the surface of eotaxin-2, the edges of the which are defined by the N-loop region and residues from the $\beta2-\beta3$ hairpin. A similar interaction surface between the CXC chemokine IL-8 and the N-terminal region of its receptor has been characterized by NMR (*11, 20*), and mutational studies have suggested the equivalent interaction may exist for CC chemokines (*12, 16*). However, this is the first report of a direct observation of such an interaction for a CC chemokine. The spectral changes observed here further suggest that the peptide extends from one end of the cleft, making contacts with the N-terminal region of the chemokine, and from the other end, making contacts with either the N-terminus or one edge of the α-helix. Thus, the peptide can be considered to wrap around the chemokine structure, interacting with almost all of the secondary structure elements as well as the N-loop and the N-terminus.

According to the two-site model for chemokine receptor activation (*17, 18*), the initial step of the interaction is binding of the N-terminal region of the receptor to the N-loop region of the chemokine (i.e., the primary interaction probed in the current peptide binding experiments), whereas the second step involves formation of an interaction between the N-terminal region of the chemokine and an as yet unidentified region of the receptor, presumably a cleft located between the transmembrane helices and/or their attached extracellular loops. The latter interaction implies that the transmembrane region of the receptor is most likely located at the bottom end of the chemokine as depicted in Figures 6A and 6B, suggesting that the N-terminal region of the receptor lies in the chemokine surface groove with its N-terminus at the top (toward the chemokine α-helix) and its C-terminus at the bottom (toward the N-terminus of the chemokine and the transmembrane bundle of the receptor). This corresponds to the orientation of the CXCR1-derived peptide bound to IL-8 in a recent solution structure (*20*).

The comparisons made here between the structures of eotaxin-2, eotaxin, and MCP-1 provide some clues as to the possible basis of receptor specificity. The N-terminal ends of the α-helices in eotaxin-2 and eotaxin extend by one and two residues, respectively, relative to MCP-1, and the peptide binding data suggest that this region of the structure may interact directly with the N-terminus of the receptor. In addition, the Lys-61 to Asp charge reversal mutation near the base of the helix suggests that negatively charged residues of the receptor might interact favorably with this region of eotaxin-2 or eotaxin but unfavorably with the same region of MCP-1. The likely importance of electrostatic interactions is further implicated by the calculated surface electrostatic potentials which are dramatically more positive for eotaxin-2 and eotaxin than for MCP-1. This difference remains apparent inside the putative receptor binding groove, suggesting that negatively charged regions of CCR3 would likely bind more tightly to the groove in eotaxin-2 and eotaxin than in MCP-1. Taken together, these observations point toward the likely role of electrostatic complementarity in controlling CCR3 recognition by CC chemokines. Future structural studies of complexes between chemokines and receptor fragments will be required to characterize the details of these interactions.

ACKNOWLEDGMENT

We thank Drs. Steven Sukits and Dimitrios Morikis for many helpful discussions regarding structure calculations, Michael Mayer for performing the activity assay and for protein purification advice, Jiqing Ye for purification of the receptor-derived peptide, Howard Woods for assistance with analytical ultracentrifugation, and Dr. Lewis Kay for providing pulse programs.

SUPPORTING INFORMATION AVAILABLE

A table summarizing the details of NMR data collection and a table listing the ^{1}H, ^{15}N, and ^{13}C chemical shifts of eotaxin-2 (5 pages). This material is available free of charge via the Internet at http://pubs.acs.org.

REFERENCES

1. Baggiolini, M., Dewald, B., and Moser, B. (1997) *Annu. Rev. Immunol. 15*, 675−705.
2. Kelvin, D. J., Michiel, D. F., Johnston, J. A., Lloyd, A. R., Sprenger, H., Oppenheim, J. J., and Wang, J.-M. (1993) *J. Leukocyte Biol. 54*, 604−612.
3. Feng, Y., Broder, C. C., Kennedy, P. E., and Berger, E. A. (1996) *Science 272*, 872−877.
4. Wells, T. N. C., Proudfoot, A. E. I., Power, C. A., and Marsh, M. (1996) *Chem. Biol. 3*, 603−609.
5. Ward, S. G., and Westwick, J. (1998) *Biochem. J. 333*, 457−470.
6. Doms, R. W., and Peiper, S. C. (1997) *Virology 235*, 179−190.
7. Cocchi, F., DeVico, A. L., Garzino-Demo, A., Arya, S. A., Gallo, R. C., and Lusso, P. (1995) *Science 270*, 1811−1815.
8. Bazan, J. F., Bacon, K. B., Hardiman, G., Wang, W., Soo, K., Rossi, D., Greaves, D. R., Zlotnik, A., and Schall, T. J. (1997) *Nature 385*, 640−644.
9. Kelner, G. S., Kennedy, J., Bacon, K. B., Kleyensteuber, S., Largaespada, D. A., Jenkins, N. A., Copeland, N. G., Bazan, J. F., Moore, K. W., Schall, T. J., and Zlotnik, A. (1994) *Science 266*, 1395−1399.
10. Stone, M. J., and Mayer, K. L. (1999) in *Chemokines in Allergic Disease* (Rothenberg, M. E., Ed.) pp 67−94, Marcel Dekker, New York.

11. Clubb, R. T., Omichinski, J. G., Clore, G. M., and Gronenborn, A. M. (1994) *FEBS Lett. 338*, 93−97.
12. Hemmerich, S., Paavola, C., Bloom, A., Bhakta, S., Freedman, R., Grunberger, D., Krstenansky, J., Lee, S., McCarley, D., Mulkins, M., Wong, B., Pease, J., Mizoue, L., Mirzadegan, T., Polsky, I., Thompson, K., Handel, T. M., and Jarnagin, K. (1999) *Biochemistry 38*, 13013−13025.
13. Struyf, S., Proost, P., Schols, D., De Clercq, E., Opdenakker, G., Lenaerts, J. P., Detheux, M., Parmentier, M., De, M. I, Scharpe, S., and Van Damme, J. (1999) *J. Immunol. 162*, 4903−4909.
14. Gong, J.-H., and Clark-Lewis, I. (1995) *J. Exp. Med. 181*, 631−640.
15. Clark-Lewis, I., Schumacher, C., Baggiolini, M., and Moser, B. (1991) *J. Biol. Chem. 266*, 23128−23134.
16. Pakianathan, D. R., Kuta, E. G., Artis, D. R., Skelton, N. J., and Hebert, C. A. (1997) *Biochemistry 36*, 9642−9648.
17. Crump, M. P., Gong, J. H., Loetscher, P., Rajarathnam, K., Amara, A., Arenzana-Seisdedos, F., Virelizier, J. L., Baggiolini, M., Sykes, B. D., and Clark-Lewis, I. (1997) *EMBO J. 16*, 6996−7007.
18. Wells, T. N. C., Power, C. A., Lustinarasimhan, M., Hoogewerf, A. J., Cooke, R. M., Chung, C. W., Peitsch, M. C., and Proudfoot, A. E. I. (1996) *J. Leukocyte Biol. 59*, 53−60.
19. Zhang, Y. J., and Rollins, B. J. (1995) *Mol. Cell. Biol. 15* (9), 4851−4855.
20. Skelton, N. J., Quan, C., Reilly, D., and Lowman, H. (1999) *Structure Folding Des. 7*, 157−168.
21. Rollins, B. (2000) *Blood 90*, 909−928.
22. Jose, P. J., Griffiths-Johnson, D. A., Collins, P. D., Walsh, D. T., Moqbel, R., Totty, N. F., Truong, O., Hsuan, J. J., and Williams, T. J. (1994) *J. Exp. Med. 179*, 881−887.
23. Forssmann, U., Uguccioni, M., Loetscher, P., Dahinden, C. A., Langen, H., Thelen, M., and Baggiolini, M. (1997) *J. Exp. Med. 185*, 2171−2176.
24. Kitaura, M., Suzuki, N., Imai, T., Takagi, S., Suzuki, R., Nakajima, T., Hirai, K., Nomiyama, H., and Yoshie, O. (1999) *J Biol. Chem. 274*, 27975−27980.
25. Ponath, P. D., Qin, S. X., Post, T. W., Wang, J., Wu, L., Gerard, N. P., Newman, W., Gerard, C., and Mackay, C. R. (1996) *J. Exp. Med. 183*, 2437−2448.
26. Daugherty, B. L., Siciliano, S. J., Demartino, J. A., Malkowitz, L., Sirotina, A., and Springer, M. S. (1996) *J. Exp. Med. 183*, 2349−2354.
27. Jas, G. S., Wang, Y., Pauls, S. W., Johnson, C. K., and Kuczera, K. (1997) *J. Chem. Phys. 107*, 8800−8812.
28. Lian, L.-Y., Derrick, J. P., Sutcliffe, M. J., Yang, J. C., and Roberts, G. C. K. (1992) *J. Mol. Biol. 228*, 1219−1234.
29. Gabuzda, D., He, J., Ohagen, A., and Vallat, A. V. (1998) *Semin. Immunol. 10*, 203-213.
30. Lavi, E., Kolson, D. L., Ulrich, A. M., Fu, L., and Gonzalez-Scarano, F. (1998) *J. Neurovirol. 4*, 301−311.
31. Prodromou, C., and Pearl, L. H. (1992) *Protein Eng. 5*, 827−829.
32. Studier, F. W., Rosenberg, A. H., Dunn, J. J., and Dubendorff, J. W. (1990) *Methods Enzymol. 185*, 60−89.
33. Wishart, D. S., Bigam, C. G., Yao, J., Abildgaard, F., Dyson, H. J., Oldfield, E., Markley, J. L., and Sykes, B. D. (1995) *J. Biomol. NMR 6*, 135−140.
34. Marion, D., Ikura, M., Tschudin, R., and Bax, A. (1989) *J. Magn. Reson. 85*, 393−399.
35. Muhandiram, D. R. and Kay, L. E. (1994) *J. Magn. Reson. 103*, 203-216.
36. Kay, L. E., Keifer, P., and Saarinen, T. (1992) *J. Am. Chem. Soc. 114*, 10663−10665.
37. Wittekind, M., and Mueller, L. (1993) *J. Magn. Reson. B 101*, 201−205.
38. Grzesiek, S., and Bax, A. (1993) *J. Biomol. NMR 3*, 185−204.
39. Zhang, O., Kay, L. E., Olivier, J. P., and Forman-Kay, J. D. (1994) *J. Biomol. NMR 4*, 845−858.
40. Grzesiek, S., Anglister, J., and Bax, A. (1993) *J. Magn. Reson. B 101*, 114−119.
41. Montelione, G. T., Lyons, B. A., Emerson, S. D., and Tashiro, M. (1992) *J. Am. Chem. Soc. 114*, 10974−10975.
42. Kay, L. E., Xu, G. Y., Singer, A. U., Muhandiram, D. R., and Forman-Kay, J. D. (1993) *J. Magn. Reson. B 101*, 333−337.
43. Yamazaki, T., Forman-Kay, J. D., and Kay, L. E. (1993) *J. Am. Chem. Soc. 115*, 11054−11055.
44. Farrow, N. A., Muhandiram, R., Singer, A. U., Pascal, S. M., Kay, C. M., Gish, G., Shoelson, S. E., Pawson, T., Forman-Kay, J. D., and Kay, L. E. (1994) *Biochemistry 33*, 5984−6003.
45. Pascal, S. M., Muhandiram, D. R., Yamazaki, T., Forman-Kay, J. D., and Kay, L. E. (1994) *J. Magn. Reson. B 103*, 197−201.
46. Vuister, G. W., Clore, G. M., Gronenborn, A. M., Powers, R., Garrett, D. S., Tschudin, R., and Bax, A. (1993) *J. Magn. Reson. B 101*, 210−213.
47. Wüthrich, K. (1986) *NMR of Proteins and Nucleic Acids*, Wiley, New York.
48. Kuboniwa, H., Grzesiek, S., Delaglio, F., and Bax, A. (1994) *J. Biomol. NMR 4*, 871−878.
49. Vuister, G. W., and Bax, A. (1993) *J. Am. Chem. Soc. 115*, 7772−7777.
50. Clubb, R. T., Ferguson, S. B., Walsh, C. T., and Wagner, G. (1994) *Biochemistry 33*, 2761−2772.
51. Grzesiek, S., Kuboniwa, H., Hinck, A. P., and Bax, A. (1995) *J. Am. Chem. Soc. 117*, 5312−5315.
52. Kraulis, J., Clore, G. M., Nilges, M., Jones, T. A., Pettersson, G., Knowles, J., and Gronenborn, A. M. (1989) *Biochemistry 28*, 7241−7257.
53. Neri, D., Szyperski, T., Otting, G., Senn, H., and Wüthrich, K. (1989) *Biochemistry 28*, 7510−7516.
54. Nilges, M., Clore, G. M., and Gronenborn, A. M. (1988) *FEBS Lett. 229*, 317−324.
55. Nilges, M., Kuszewski, J., and Brünger, A. T. (1991) in *Computational Aspects of the Study of Biological Macromolecules by NMR* (Hoch, J. C., Ed.) pp 451−455, Plenum Press, New York.
56. Kuszewski, J., Nilges, M., and Brünger, A. T. (1992) *J Biomol. NMR 2*, 33−56.
57. Brünger, A. T. (1993) *X-PLOR Version 3.1 A System for X-ray Crystallography and NMR*, Yale University Press, New Haven.
58. Laskowski, R. A., Rullmannn, J. A., MacArthur, M. W., Kaptein, R., and Thornton, J. M. (1996) *J. Biomol. NMR 8*, 477−486.
59. Vriend, G. (1990) *J. Mol. Graph. 8*, 52−56.
60. Vriend, G., and Sander, C. (1993) *J. Appl. Crystallogr. 26*, 47−60.
61. Berman, H. M., Westbrook, J., Feng, Z., Gilliland, G., Bhat, T. N., Weissig, H., Shindyalov, I. N., and Bourne, P. E. (2000) *Nucleic Acids Res. 28*, 235−242.
62. He, J., and Landau, N. R. (1995) *J. Virol. 69*, 4587−4592.
63. Deng, H., Liu, R., Ellmeier, W., Choe, S., Unutmaz, D., Burkhart, M., Di Marzio, P., Marmon, S., Sutton, R. E., Hill, C. M., Davis, C. B., Peiper, S. C., Schall, T. J., Littman, D. R., and Landau, N. R. (1996) *Nature 381*, 661−666.
64. Ralston, G. (1993) *Introduction to Analytical Ultracentrifugation*, Beckman Instruments, Fullerton, CA.
65. Crump, M. P., Rajarathnam, K., Kim, K. S., Clark-Lewis, I., and Sykes, B. D. (1998) *J. Biol. Chem. 273*, 22471−22479.
66. Richardson, J. S. (1981) *Adv. Protein Chem. 34*, 167−223.
67. Mizoue, L. S., Bazan, J. F., Johnson, E. C., and Handel, T. M. (1999) *Biochemistry 38*, 1402−1414.
68. Ye, J., Mayer, K. L., and Stone, M. J. (1999) *J. Biomol. NMR 15*, 115−124.
69. Crump, M. P., Spyracopoulos, L., Lavigne, P., Kim, K. S., Clark-Lewis, I., and Sykes, B. D. (1999) *Protein Sci. 8*, 2041−2054.
70. LiWang, A. C., Cao, J. J., Zheng, H., Lu, Z., Peiper, S. C., and LiWang, P. J. (1999) *Biochemistry 38*, 442−453.
71. Handel, T. M. and Domaille, P. J. (1996) *Biochemistry 35*, 6569−6584.
72. Lubkowski, J., Bujacz, G., Boque, L., Domaille, P. J., Handel, T. M., and Wlodawer, A. (1997) *Nat. Struct. Biol. 4*, 64−69.

73. Kim, K. S., Rajarathnam, K., Clark-Lewis, I., and Sykes, B. D. (1996) *FEBS Lett. 395*, 277−282.
74. Meunier, S., Bernassau, J. M., Guillemot, J. C., Ferrara, P., and Darbon, H. (1997) *Biochemistry 36*, 4412−4422.
75. Paolini, J. F., Willard, D., Consler, T., Luther, M., and Krangel, M. S. (1994) *J. Immunol. 153*, 2704−2717.
76. Sticht, H., Escher, S. E., Schweimer, K., Forssmann, W. G., Rosch, P., and Adermann, K. (1999) *Biochemistry 38*, 5995−6002.
77. Rajarathnam, K., Sykes, B. D., Kay, C. M., Dewald, B., Geiser, T., Baggiolini, M., and Clark-Lewis, I. (1994) *Science 264*, 90−92.
78. Rajarathnam, K., Kay, C. M., Dewald, B., Wolf, M., Baggiolini, M., Clark-Lewis, I., and Sykes, B. D. (1997) *J. Biol. Chem. 272* (3), 1725−1729.
79. Lowman, H. B., Fairbrother, W. J., Slagle, P. H., Kabakoff, R., Liu, J., Shire, S., and Hebert, C. A. (1997) *Protein Sci. 6*, 598−608.
80. Hoogewerf, A., Kuschert, G. S. V., Proudfoot, A. E. I., Borlat, F., Clark-Lewis, I., Power, C. A., and Wells, T. N. C. (1997) *Biochemistry 36*, 13570−13578.
81. Laurence, J. S., LiWang, A. C., and LiWang, P. J. (1998) *Biochemistry 37*, 9346−9354.
82. Lavery, R., and Pullman, B. (1985) *J. Biomol. Struct. Dyn. 2*, 1021−1032.
83. Wishart, D. S., Sykes, B. D., and Richards, F. M. (1992) *Biochemistry 31*, 1647−1651.
84. Wishart, D. S. and Sykes, B. D. (1994) *J. Biomol. NMR 4*, 171−180.
85. Shuker, S. B., Hajduk, P. J., Meadows, R. P., and Fesik, S. W. (1996) *Science 274*, 1531−1534.
86. Koradi, R., Billeter, M., and Wüthrich, K. (1996) *J. Mol. Graphics 14*, 51−55.

BI000523J